Optomechanical sideband cooling of a micromechanical oscillator close to the quantum ground state

R. Rivière,[1] S. Deléglise,[1,2] S. Weis,[1,2] E. Gavartin,[2] O. Arcizet,[3] A. Schliesser,[1,2] and T. J. Kippenberg[1,2,*]

[1]*Max Planck Institut für Quantenoptik, DE-85748 Garching, Germany*

[2]*École Polytechnique Fédérale de Lausanne (EPFL), CH-1015 Lausanne, Switzerland*

[3]*Institut Néel-CNRS/Université Joseph Fourier, FR-38042 Grenoble, France*

(Received 31 October 2010; published 24 June 2011)

Cooling a mesoscopic mechanical oscillator to its quantum ground state is elementary for the preparation and control of quantum states of mechanical objects. Here, we pre-cool a 70-MHz micromechanical silica oscillator to an occupancy below 200 quanta by thermalizing it with a 600-mK cold ^{3}He gas. Two-level-system induced damping via structural defect states is shown to be strongly reduced and simultaneously serves as a thermometry method to independently quantify excess heating due to the cooling laser. We demonstrate that dynamical back action optical sideband cooling can reduce the average occupancy to 9 ± 1 quanta, implying that the mechanical oscillator can be found $(10 \pm 1)\%$ of the time in its quantum ground state.

DOI: 10.1103/PhysRevA.83.063835 PACS number(s): 42.50.Pq, 42.50.Wk, 42.65.Sf, 03.65.Ta

I. INTRODUCTION

The quantum regime of macroscopic mechanical systems has received significant interest over the past decade [1–4]. Mechanical systems cooled to the quantum ground state may allow probing quantum-mechanical phenomena on an unprecedentedly large scale, could enable quantum-state preparation of mechanical systems, and have been proposed as an interface between photons and stationary qubits [5]. To achieve ground-state cooling, two challenges have to be met: first, most mechanical oscillators have vibrational frequencies $\Omega_m/(2\pi) < 100$ MHz, such that low mode temperatures $T_{\rm eff}$ are required to achieve $\hbar\Omega_m > k_B T_{\rm eff}$ ($\hbar$ is the reduced Planck constant and k_B is the Boltzmann constant). Second, quantum-limited measurements of mechanical motion must be performed at the level of the zero point motion $x_{\rm zpf} = \sqrt{\hbar/(2m_{\rm eff}\Omega_m)}$ in order to probe the state of the oscillator of mass $m_{\rm eff}$.

Recently, a piezomechanical oscillator has been cooled to the quantum regime [6]. Due to its GHz resonance frequency, conventional cryogenics could be employed for cooling while it was probed using its piezoelectrical coupling to a superconducting qubit. In contrast, cooling schemes based on dynamical backaction [7,8] can be applied to a much wider class of nanomechanical and micromechanical oscillators. Following the observation of optical cooling based on a photothermal effect [9], dynamical backaction cooling by radiation pressure [10–13], as predicted more than 40 years ago [7], was demonstrated. This scheme is based on parametric coupling of an optical and mechanical resonance and simultaneously allows sensitive detection of mechanical motion. In analogy to the case of trapped ions, in which sideband cooling has led to the preparation of the vibrational ground state [14], dynamical backaction sideband cooling has been theoretically shown to allow reaching the quantum ground state of a mechanical mode [15–17].

Despite major progress, ground-state cooling using this approach has remained challenging, owing to insufficiently low starting temperatures and/or excess heating by the electromagnetic field used for cooling [18–20]. Here, we demonstrate an experimental optomechanical setting that successfully addresses these challenges and achieve cooling to only 9 ± 1 quanta, implying that the oscillator resides $10 \pm 1\%$ of its time in the quantum ground state. Our experiment operates in the temperature regime below 1 K, where the coupling of the mechanical mode to two-level systems (TLS) induces significant mechanical dissipation. The temperature-dependent effects of TLS in glass can be harnessed for an independent thermometry method, in addition to conventional noise thermometry of the mechanical modes. Using two independent methods for the determination of the mechanical oscillator's temperature, we are able to reliably quantify resonant and off-resonant heating by the cooling laser. Our measurements demonstrate that resonant heating is negligible for the chosen experimental system, enabling a wide range of future experiments in quantum optomechanics.

II. EXPERIMENT

We use silica toroidal resonators, which support whispering gallery modes (WGM) of ultrahigh finesse co-located with a low-loss mechanical radial breathing mode (RBM) [21,22] and large mutual optomechanical coupling. The devices used here have been optimized for narrow optical linewidths κ, and moderately high mechanical frequencies Ω_m, thereby operating deeply in the resolved sideband (RSB) regime ($\Omega_m \approx 2\pi \times 70\,\text{MHz} \gtrsim 10\kappa$), while at the same time the pillar geometry was engineered for low mechanical dissipation [23,24] (Fig. 1).

For the cryogenic laser cooling experiments, we subject these samples directly to a ^{3}He gas evaporated from a reservoir of liquid ^{3}He. At a pressure of $\sim$0.7 mbar, the gas provides a thermal bath at a temperature of about 600 mK. However, it is essential to verify thermalization of the toroid to the exchange gas. To this end, a low-noise fiber laser is coupled to a WGM through a fiber taper positioned in the near field of the mode via piezoelectric actuators (Attocube Systems AG). The displacement fluctuations of the RBM can be extracted and used to infer its noise temperature [25,26]. As shown in Fig. 1(b), it follows the temperature of the helium gas down to temperatures of 600 mK for weak probing (i.e., $< 1\ \mu$W input laser power).

*tobias.kippenberg@epfl.ch

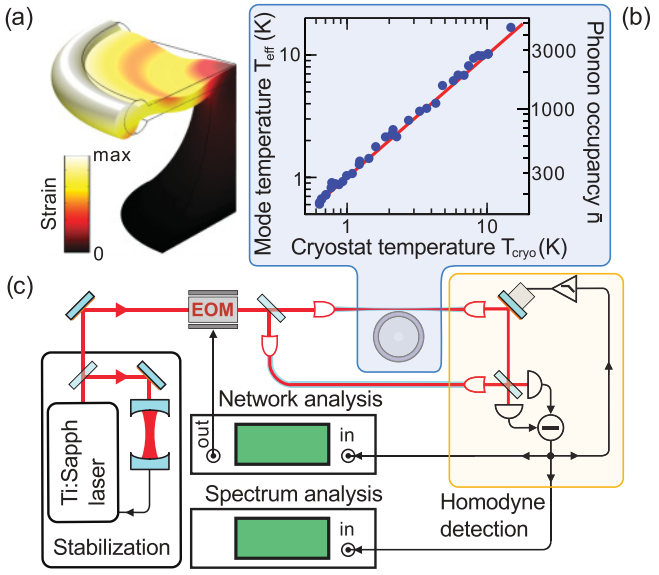

FIG. 1. (Color online) Cooling a micromechanical oscillator. (a) High-Q mechanical and optical modes are co-located in a silica microtoroid. The simulated displacement pattern of the mechanical radial breathing mode (RBM) is shown. The optical whispering gallery mode (WGM) is confined to the rim. (b) Thermalization of the RBM to the temperature of the ^{3}He gas, with the lowest achieved temperature corresponding to a mean occupancy of the RBM below 200 quanta. (c) Optical setup used for displacement monitoring of the mechanical mode, based on homodyne analysis of the light re-emerging from the toroid's WGM (see text for detailed description).

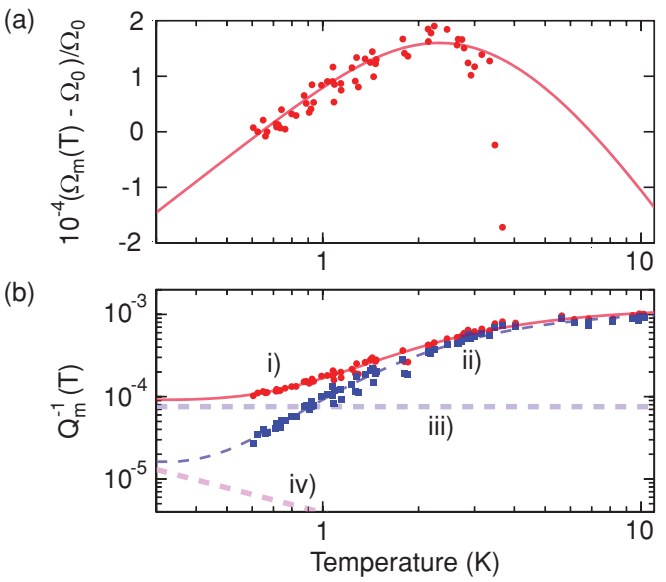

FIG. 2. (Color online) TLS-induced change of the resonance frequency [$\Omega_m(T)$] (a) and inverse mechanical quality factor [$Q_m^{-1}(T)$] (b) of the radial breathing mode. Measured data (points) agree well with the models (solid lines) described in Eqs. (1) and (2). Subtraction of the temperature-independent clamping damping (line iii) yields the theoretically possible material-limited damping values (squares and line ii). At very low temperatures, damping by resonant interaction with TLS (line iv) would be dominant. Ω_0 is the mechanical angular frequency $\Omega_m(T)$ measured at the arbitrary temperature $T = 620$ mK. The model parameters are given in Appendix A.

For optomechanical sideband cooling, we employed a frequency-stabilized Ti:sapphire laser and a homodyne detection scheme [18] for quantum-limited detection of mechanical displacement fluctuations [Fig. 1(c)]. Spectral analysis of the homodyne signal provides direct access to the mechanical displacement spectrum, from which the mechanical damping and resonance frequency can be extracted. The spectra are calibrated in absolute terms by applying a known frequency modulation to the laser using an electro-optic modulator (EOM) as detailed in Refs. [18,26]. After the acquisition of each spectrum, the precise detuning of the laser from the cavity resonance is determined by sweeping the modulation frequency of the EOM and recording the demodulated homodyne signal with a network analyzer [27].

The independent thermometry method we are presenting is based on the strong temperature dependence of the material's mechanical properties caused by the presence of structural defects modeled as two-level systems [25,28]. Relaxation of the TLS under excitation from an acoustic wave modifies the mechanical susceptibility, leading to a change in mechanical resonance frequency Ω_m and a change of the damping rate $\Gamma_m = \Omega_m/Q_m$ (with the mechanical quality factor Q_m).

Two different relaxation regimes have to be considered (cf. Appendix A) for sample temperatures T between 0.6 and 3 K: tunneling-assisted relaxation [29,30] and single-phonon resonant interaction [30]. Thermally activated relaxation [31] dominates the frequency shift at temperatures above 3 K, but is negligible in the temperature range at which the laser cooling experiments are performed. In the presence of tunneling relaxation ("tun") and resonant interactions ("res"), the mechanical oscillator properties can be expressed as

$$\Omega_m(T) = \Omega_{upt} + \delta\Omega_{tun}(T) + \delta\Omega_{res}(T), \quad (1)$$

$$Q_m^{-1}(T) = Q_{cla}^{-1} + Q_{tun}^{-1}(T) + Q_{res}^{-1}(T), \quad (2)$$

where Ω_{upt} is the unperturbed angular frequency in the absence of TLS-induced effects and $\Omega_m Q_{cla}^{-1}$ is the damping rate due to the clamping of the resonator to the substrate, dominating Γ_m at room temperature. For readability, we simply take $\Omega_m = \Omega_m(T_{cryo})$ with T_{cryo} being the independently measured temperature crysotat, when the TLS-induced thermal dependence of the frequency is quantitatively neglected over the temperature range of interest (relative shift of the order of 10^{-4}). For the damping however, since the TLS significantly alter its value, the short notation $Q_m = Q_m(T)$ and $\Gamma_m = \Gamma_m(T)$ still signifies that the thermal dependence is taken into account. The respective temperature dependencies in the relevant regimes of TLS damping are detailed in Appendix A. In contrast to previous experiments using ^{4}He [18,19], where Q_m was limited to ~3000 at $T \approx 3$ K due to TLS damping, Q_m reaches values exceeding 10^4 with significant contributions from clamping losses for the lowest temperatures of 600 mK. Such values are sufficient to enable ground-state cooling since $Q_m/\bar{n}_i \gg 1$ and $\bar{n}_i\Omega_m/Q_m \ll \kappa$ ($\bar{n}_i$ is the initial occupancy) [32]. The temperature dependence of the mechanical Q is in excellent quantitative agreement with the one caused by TLS defects (Fig. 2). This well-understood temperature dependence of the TLS-induced effects [Eqs. (1) and (2)] enables its use as a

"thermometer" of the sample temperature T after a calibration measurement, as shown in Fig. 2, has been performed once. Importantly, this method can reveal excess heating by the cooling laser.

III. RESULTS

We studied optomechanical cooling [10–12] by performing a series of experiments in which mechanical displacement noise spectra were recorded while varying the laser detuning $\bar{\Delta} \equiv \omega_l - \bar{\omega}_c$. Here, ω_l is the laser's (angular) frequency and $\bar{\omega}_c$ is the WGM frequency (cf. Appendix B). To model radiation-pressure-induced dynamical backaction [7] for the present microresonators, we take into account that backscattering of light couples modes $a_{\circlearrowleft}$ and $a_{\circlearrowright}$ with opposite circulation sense [33,34]. This lifts the degeneracy between the system's eigenmodes $a_\pm = (a_{\circlearrowleft} \pm a_{\circlearrowright})/\sqrt{2}$, the resonance frequencies of which are split by the scattering coupling rate γ. During a detuning series as reported here, both modes are populated with a mean field $\bar{a}_\pm = \sqrt{\kappa_{ex}/2}\, L_\pm(\bar{\Delta}) s_{in}$, where $P_{in} = |s_{in}|^2 \hbar\omega_l$ is the driving laser power, κ_{ex} is the coupling rate to the fiber taper, $|\bar{a}_\pm|^2$ is the mean photon population in the new eigenmodes, and $L_\pm(\bar{\Delta}) \equiv [-i(\bar{\Delta} \pm \gamma/2) + \kappa/2]^{-1}$ is the modes' Lorentzian response.

In the context of cavity optomechanics, it is important to realize that three-mode interactions [35] can be neglected in the present configuration (cf. Appendix B). The radiation pressure forces induced by the light in these modes can therefore simply be added. The usual linearization procedure [36,37] then yields an inverse effective mechanical susceptibility

$$[\chi_{eff}(\Omega)]^{-1} = [\chi_m(\Omega)]^{-1} - i\Omega_m m_{eff} f(\Omega), \tag{3}$$

in which the bare mechanical susceptibility $\chi_m(\Omega)$ is modified by the dynamical backaction term

$$f(\Omega) = 2g_0^2 \sum_{\sigma=\pm} |\bar{a}_\sigma|^2 \{L_\sigma(\bar{\Delta} + \Omega) - [L_\sigma(\bar{\Delta} - \Omega)]^*\} \tag{4}$$

with the vacuum optomechanical coupling rate [26] $g_0 \equiv G x_{zpf}$ and $G = d\omega_c/dx$. For moderate driving powers [32], the susceptibility of the mechanical mode is the one of a harmonic oscillator with effective damping rate and resonance frequency of

$$\Gamma_{eff} \approx \Gamma_m(T) + \mathrm{Re}[f(\Omega_m)], \tag{5}$$

$$\Omega_{eff} \approx \Omega_m(T) + \mathrm{Im}[f(\Omega_m)]/2. \tag{6}$$

For the sample of radius $R \approx 25\ \mu$m studied in the following, a coupling rate of $|g_0| \approx 2\pi \times (1.2 \pm 0.2)$ kHz is determined from the coupling parameter $|G| = \omega_c/R \approx 2\pi \times 16$ GHz/nm and effective mass $m_{eff} = 20 \pm 5$ ng. Figure 3 shows the results of a detuning series, which was taken with an input laser power of 2 mW, with the temperature of the ^{3}He gas stabilized to $T_{cryo} = 850$ mK at a pressure of 2.8 mbar. We found it necessary to give more weight in the coupled fit to the optical spring effect (relative weight 0.9) than the damping rate, since the mechanical resonance frequency can be extracted from the spectra with higher accuracy than the damping rate. The obtained fit parameters κ, γ, and s_{in} are found to be in good agreement with independent results deduced from the frequency modulation measurement

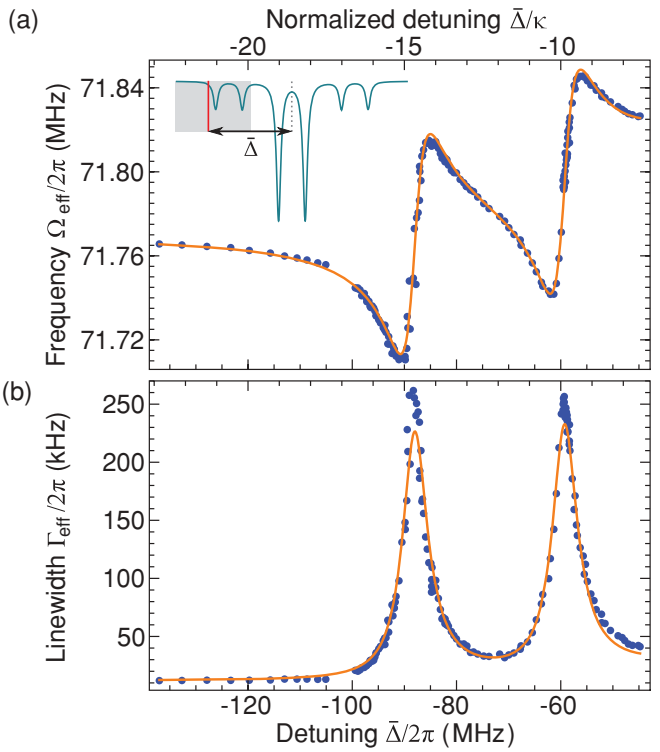

FIG. 3. (Color online) (a) Effective resonance frequency and (b) linewidth of the RBM when a 2-mW power laser is tuned through the lower mechanical sideband of the split optical mode (inset). Points are measured data extracted from the recorded spectra of thermally induced mechanical displacement fluctuations, and solid lines are a coupled fit using the model of Eqs. (1)–(6), taking into account resonant and off-resonant (stray light) heating, modifying temperature-dependent damping and frequency shift caused by the TLS.

($\kappa \approx 2\pi \times 6$ MHz, $\gamma \approx 2\pi \times 30$ MHz) and the measured laser power.

The excellent quality of the fit, together with the measured temperature dependence of the TLS effects on the mechanical mode, furthermore, allows us to extract the temperature T of the sample. Importantly, for large detunings $|\bar{\Delta}| \gg \kappa$, the TLS thermometer reveals (via a decrease of the mechanical quality factor to $Q_m = 5970$) an increase of the sample temperature by $\delta T_{stray} \approx 220$ mK, which we attribute to heating induced by absorbed stray light scattered from defects on the taper fiber, which were observed to aggregate upon its production. As the laser is tuned closer to resonance, more light is coupled into the WGM, leading to the appearance of an additional (detuning-dependent) temperature increase

$$T \approx T_{cryo} + \delta T_{stray} + \delta T_{WGM}. \tag{7}$$

Here, $\delta T_{WGM} = \beta \kappa_{abs} (|a_+|^2 + |a_-|^2) \hbar\omega_l$ denotes the increase in temperature following the cavity's double-Lorentzian absorption profile, $\kappa_{abs} \lesssim \kappa - \kappa_{ex}$ is the photon absorption rate, and β is the temperature increase per absorbed power. This heating term will lead via the TLS-dependent mechanical susceptibility (cf. Fig. 2) to additional changes in Γ_{eff} and Ω_{eff} in the detuning series (cf. Fig. 3), from which the amount of additional resonant heating (δT_{WGM}) can be extracted. Applying this procedure to the data yields a temperature increase of $\delta T_{WGM} \approx 70$ mK on the lower sideband (i.e., for

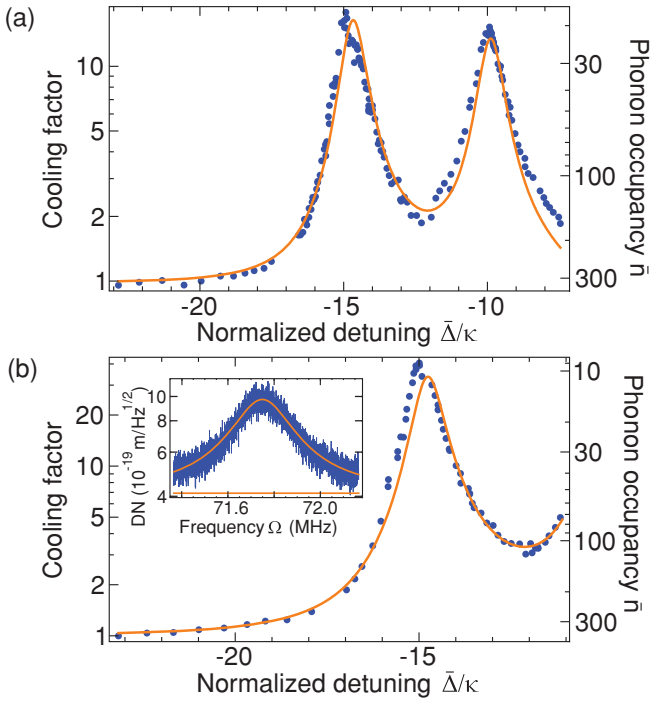

FIG. 4. (Color online) Cooling factor $(T_{\rm cryo}+\delta T_{\rm stray})/T_{\rm eff}$ and phonon occupancy of the RBM vs laser detuning $\bar{\Delta}$ for (a) $P_{\rm in}=2$ mW and (b) $P_{\rm in}=4$ mW. Points are phonon occupancies derived from the measured noise temperature, while solid lines correspond to the occupancies expected from the dependency of sample temperature and (intrinsic and effective) damping extracted from the detuning series as shown in Fig. 3. A minimum phonon number of $\bar{n}=9\pm1$ is obtained. The inset shows a mechanical displacement noise (DN) spectrum at the optimum detuning ($\bar{\Delta}=\bar{\Delta}_{\rm opt}$), illustrating the high signal-to-noise ratio achieved despite the low occupancy for $P_{\rm in}=2$ mW.

$\bar{\Delta}=-\Omega_{\rm m}-\gamma/2$ corresponding to the optimum detuning $\bar{\Delta}_{\rm opt}$ in the deep RSB regime). This modest increase can be explained by the large sideband factor [23], which implies that only little optical power ($\sim\kappa_{\rm abs}|a_+|^2\hbar\omega_{\rm l}\lesssim P_{\rm in}/1300$) can be absorbed in the cavity when $\bar{\Delta}=\bar{\Delta}_{\rm opt}$. Importantly, we can test the consistency of the derived detuning-dependent quantities [T, $\Gamma_{\rm m}(T)$, and $\Gamma_{\rm eff}$] by comparing the expected effective temperature of the RBM due to optomechanical cooling, i.e., $T_{\rm eff}=T\cdot\Gamma_{\rm m}(T)/\Gamma_{\rm eff}$, with the effective temperature derived from noise thermometry via integration of the calibrated noise spectra [18].

Figure 4(a) shows this comparison for the detuning series discussed above. Using the model of Eqs. (2)–(6), adjusted to the data of Fig. 3, we obtain good agreement for the effective temperatures obtained in both ways. To achieve this level of agreement, it is necessary to take into account the optomechanical deamplification [38] of the laser phase modulation used for calibrating the mechanical fluctuation spectra in absolute terms.

Figure 4(b) shows the same comparison for a cooling run at a high laser power (4 mW), for which we observe slightly increased heating by $\delta T_{\rm stray}\approx400$ mK, while additional heating by $\delta T_{\rm WGM}$ could not be discerned in this measurement. In spite of the reduced mechanical quality factor $Q_{\rm m}(T_{\rm cryo}+\delta T_{\rm stray})=4880$, the lowest extracted occupancy is $\bar{n}=10$ according to the detuning series fit. The lowest inferred *noise* temperature of a single measurement is even slightly lower, corresponding to $\bar{n}=9\pm1$, where the uncertainty is dominated by systematic errors, which we estimate from the deviations of the effective temperature derived in the two independent ways described above. Note that this occupancy implies already a probability of $P(n=0)=(1+\bar{n})^{-1}=(10\pm1)\%$ to find the oscillator in its quantum ground state. From this measurement, we can also extract an imprecision-backaction product [18] (cf. Appendix C for detailed derivations) of $\sqrt{S_{xx}^{\rm im}S_{FF}}=(49\pm8)\hbar/2$ if the total Langevin force noise is (conservatively) considered as measurement backaction. Due to the resolved-sideband operation, force noise coming from quantum backaction (as yet only observed on cold atomic gases [39]) is expected to be nearly two orders of magnitude weaker and therefore negligible.

IV. CONCLUSION

We have cooled a mechanical oscillator using a combination of cryogenic ^{3}He exchange gas pre-cooling and optomechanical sideband cooling [23] to 9 ± 1 quanta, implying that the mechanical oscillator occupies the ground state $10\pm1\%$ of the time. This is the lowest phonon occupancy that has been achieved with optomechanical sideband cooling so far. It is possible to populate the quantum ground state with higher probability by avoiding excess heating due to fiber contamination, by using higher cooling laser powers and by improving $g_0^2/\Gamma_{\rm m}$, which can be achieved by engineering mechanical modes [24] for lower mass and clamping losses. Simultaneously, such a system bears promise to give access to the regime of strong optomechanical coupling [32,40] in which the coherent coupling rate $\sqrt{\bar{n}_{\rm p}}g_0$ exceeds the cavity decay rate κ and the thermal decoherence rate $k_{\rm B}T/(\hbar Q_{\rm m})$ of $2\pi\times2.6$ MHz in the present experiment ($\bar{n}_{\rm p}$ is the average cavity photon number). For occupancies $\bar{n}\lesssim1$, individually resolved anti-Stokes and Stokes sidebands [15,23] of an independent resonant readout laser will display a measurable asymmetry of $\bar{n}/(\bar{n}+1)$ arising from the nonzero commutator of the ladder operators describing the mechanical harmonic oscillator in quantum terms. In addition, the described system may give experimental access to the regime where quantum backaction becomes comparable or exceeds thermal noise, allowing pondermotive squeezing [36] or QND photon measurements.

ACKNOWLEDGMENTS

T.J.K. acknowledges funding by an ERC Starting Grant SiMP, the EU (Minos), the DARPA/MTO ORCHID program, and the NCCR of Quantum Photonics. S.D. is funded by a Marie Curie IEF. The MPQ is acknowledged for hosting this experiment. All authors thank Ewold Verhagen for the finite element method simulation and Pierre Verlot for stimulating discussions. R.R., S.D., and S.W. conducted the experiment.

APPENDIX A: TWO-LEVEL SYSTEMS

Tunneling systems in SiO_2 play an important role in cryogenic operation of silica mechanical oscillators. They lead to a temperature-dependent frequency shift (via a change

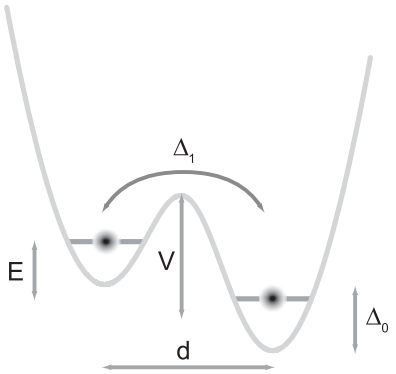

FIG. 5. Double-well potential with relevant levels and naming convention.

in speed of sound) of the considered mechanical mode and temperature-dependent mechanical quality factor. We will discuss these effects in the following and give the relevant formulas that have been used to fit the data in the main part of the manuscript. An extensive study of TLS effects can be found in Refs. [28,30] and we summarize here the essential results.

As first considered by L. Pauling in 1930 [41], tunneling of atoms occurs in solids with a certain degree of disorder where, in the local environment of an atomic site, several potential minima exist. This can be the case in the vicinity of defects in crystals or, more frequently, in amorphous materials. For amorphous solids at low temperatures, the tunneling dynamics can be well captured in a simple model consisting of an ensemble of two-level systems, each of which is described by a generic double-well potential (Fig. 5). This potential is parametrized only by the barrier height V, the initial energy asymmetry Δ_0, and the spatial separation between the two potential minima d. A tunneling coupling strength

$$\Delta_1 = \hbar\Omega_1 e^{-\lambda} \tag{A1}$$

with the intrinsic oscillation angular frequency Ω_1 within the individual atomic sites can then be deduced, with the tunneling parameter

$$\lambda \approx \sqrt{\frac{2mV}{\hbar^2}}\frac{d}{2} \tag{A2}$$

depending on the atomic mass m. Due to this tunnel coupling, the new eigenmodes of the coupled system exhibit an energy splitting of

$$E = \sqrt{\Delta_0^2 + \Delta_1^2}. \tag{A3}$$

Phonons couple to TLS via their strain field that leads to a deformation of the TLS potential (notably leading to a change in the barrier height V). As a consequence, the TLS are driven out of thermal equilibrium and relaxation processes will exchange energy with the heat bath. Transitions between the two energy levels are induced by several distinct processes that become dominant in different temperature regimes.

(i) At very low temperatures ($T \lesssim E/k_B$), the density of thermal phonons is low, such that relaxation processes only play a minor role. Here, a significant population imbalance between lower and excited state exists, and the most efficient transition mechanism is resonant absorption of phonons of a frequency $\Omega_m = E/\hbar$. This mechanism exhibits, as in the case of other two-level systems, a saturation behavior [42].

(ii) At temperatures $T \gtrsim E/k_B$ (typically a few Kelvin), the number of thermal phonons has increased to a level at which Raman processes involving a tunneling through the barrier become predominant. It is mainly this temperature range that will be relevant for the description of the phenomena seen in the present cooling experiment.

(iii) At even higher temperatures, thermally activated relaxation dominates. In this case, multiphonon processes with an excitation across the barrier take place.

1. Relaxation contribution

If relaxation is the dominant process, the general expression for the mean-free path of a phonon of frequency Ω_m is given by [28,30]

$$l^{-1}(T) = \frac{1}{\rho c_s^3}\iint\left(-\frac{\partial n_0}{\partial E}\right)4B^2\frac{\Delta_0^2}{E^2}\frac{\Omega_m^2\tau}{1+\Omega_m^2\tau^2} \times \bar{P}(\Delta_0,\lambda)\,d\Delta_0\,d\lambda. \tag{A4}$$

The integration is performed over all TLS that can interact with the phonon. Here, $\bar{P}(\Delta_0,\lambda)$ is the volume density of TLS with energy asymmetry between Δ_0 and $\Delta_0 + d\Delta_0$ and tunnel parameter between λ and $\lambda + d\lambda$,

$$n_0 = \frac{1}{e^{E/k_BT}+1} \tag{A5}$$

is the thermal equilibrium Boltzmann repartition function, c_s is the speed of sound, ρ is the mass density of the solid, τ is the relaxation time of the individual TLS, and B is the coefficient linking a deformation δe to a change of E via $\delta E = 2B(\Delta_0/E)\delta e$.

A mechanical quality factor of

$$Q_m^{-1}(T) = \frac{c_s l^{-1}(T)}{\Omega_m} \tag{A6}$$

can then be deduced. For the corresponding relative change in the speed of sound (i.e., frequency shift of a mechanical resonance), one obtains from the Kramers-Kronig relations

$$\delta\Omega_m(T) = -\frac{\Omega_m}{2\rho c_s^2}\iint\left(-\frac{\partial n_0}{\partial E}\right)4B^2\frac{\Delta_0^2}{E^2}\frac{1}{1+\Omega_m^2\tau^2} \times \bar{P}(\Delta_0,\lambda)\,d\Delta_0\,d\lambda. \tag{A7}$$

a. Tunneling-assisted relaxation

Within the framework of the so-called tunneling model [28,30], the relaxation time is given by

$$\tau = \tau_m\frac{E^2}{\Delta_1^2} \tag{A8}$$

with the maximum relaxation rate

$$\tau_m^{-1} = \frac{3}{c_s^5}\frac{B^2}{2\pi\rho\hbar^4}E^3\coth\left(\frac{E}{2k_BT}\right). \tag{A9}$$

Parametrizing the integrals in terms of the energy splitting E and the parameter $u = \tau^{-1}/\tau_{\rm m}^{-1}$ yields [28,30]

$$Q_{\rm tun}^{-1}(T) = \frac{2\bar{P}B^2}{\rho c_{\rm s}^2}\int_0^\infty\left(-\frac{\partial n_0}{\partial E}\right)\Omega_{\rm m}\tau_{\rm m}\int_0^1\frac{\sqrt{1-u}}{u^2+\Omega_{\rm m}^2\tau_{\rm m}^2}\,du\,dE \tag{A10}$$

and

$$\delta\Omega_{\rm tun}(T) = -\frac{\Omega_{\rm m}\bar{P}B^2}{\rho c_{\rm s}^2}\int_0^\infty\left(-\frac{\partial n_0}{\partial E}\right)\times\int_0^1\frac{u\sqrt{1-u}}{u^2+\Omega_{\rm m}^2\tau_{\rm m}^2}\,du\,dE, \tag{A11}$$

where it is assumed that the density $\bar{P}(E,\lambda) = \bar{P}$ is constant, which is consistent with experiments. A prominent feature in this regime is a plateau of the quality factors for temperatures of a few Kelvins with Q values of

$$Q_{\rm plateau}^{-1} = \frac{\pi}{2}\frac{\bar{P}B^2}{\rho c_{\rm s}^2}. \tag{A12}$$

b. Thermally activated relaxation

At higher temperature, the rate is given by the Arrhenius law and only depends on the energy barrier height

$$\tau_{\rm th}^{-1} = \tau_0^{-1}e^{-V/k_{\rm B}T}, \tag{A13}$$

where τ_0 represents the period of oscillation in individual wells [28,31].

2. Resonant processes

For resonant interaction between phonons and TLS, it can be shown that [28,30]

$$Q_{\rm res}^{-1}(T) = \frac{\pi\bar{P}B^2}{\rho c_{\rm s}^2}\tanh\left(\frac{\hbar\Omega_{\rm m}}{2k_{\rm B}T}\right), \tag{A14}$$

$$\delta\Omega_{\rm res}(T) = \frac{\Omega_{\rm m}\bar{P}B^2}{\rho c_{\rm s}^2}\ln\left(\frac{T}{T_0}\right), \tag{A15}$$

where T_0 is a reference temperature. While resonant processes do not significantly contribute to the mechanical quality factors in our experiment, they dominantly contribute to the frequency shift.

3. Fitting parameters for Fig. 2

The curves shown in Fig. 2 have been fitted with the equations given in the previous sections. For the frequency shift, the sum of the tunneling relaxation and the resonant contribution has been taken into account. The latter dominates this effect up to about $T = 2$ K. The contribution of thermally activated relaxation has been omitted since it does not contribute significantly in the considered temperature range. Fitting of the Q dependency has been done using the sum of tunneling relaxation, resonant contribution, and a constant offset accounting for the clamping losses ($Q_{\rm cla}^{-1}$), i.e., loss of acoustic energy due to leaking into the substrate for this particular toroid. Here, the resonant contribution plays a minor role.

For the curves shown in Fig. 2, we used the material parameters

$$c_{\rm s} = 5800\ {\rm m/s}, \quad \rho = 2330\ {\rm kg/m^3},$$

the measured resonance frequency

$$\Omega_{\rm m} = 2\pi \times 76.3\ {\rm MHz},$$

as well as the adjusted parameters

$$B = 1.1\times10^{-19}\ {\rm J},$$
$$\bar{P}_{Q_{\rm m}} = 4.6\times10^{45}\ {\rm m^{-3}},$$
$$\bar{P}_{\Omega_{\rm m}} = 2.5\times10^{45}\ {\rm m^{-3}}.$$

For the fitting of the two curves (mechanical quality factor, resonance frequency shift), two different values for $\bar{P}$ had to be used. Given that the two traces are governed by two different regimes, small differences in the density of contributing TLS to the two effects seem to be justified. The literature [43] value of the dimensionless parameter $C = \bar{P}B^2/(\rho c_s^2) = 3.010^{-4}$ shows a reasonable agreement with the parameters of the resonance frequency ($C_{\Omega_{\rm m}} = 7.110^{-4}$) and damping ($C_{Q_{\rm m}} = 3.910^{-4}$) fits.

APPENDIX B: DYNAMICAL BACKACTION IN THE PRESENCE OF MODE SPLITTING

In the framework of coupled-mode theory [44], the two coupled counterpropagating modes [33,34] in a WGM resonator can be described by the equations of motion (in a frame rotating at the laser frequency)

$$\dot{a}_{\rm ccw}(t) = \{i[\Delta - Gx(t)] - \kappa/2\}a_{\rm ccw}(t) + i\frac{\gamma}{2}a_{\rm cw}(t) + \sqrt{\eta_{\rm c}\kappa}s_{\rm in}(t), \tag{B1}$$

$$\dot{a}_{\rm cw}(t) = \{i[(\Delta - Gx(t)] - \kappa/2\}a_{\rm cw}(t) + i\frac{\gamma}{2}a_{\rm ccw}(t). \tag{B2}$$

Here, $\eta_{\rm c}$ describes the coupling parameters defined via $\eta_{\rm c} = \frac{\kappa_{\rm ex}}{\kappa_{\rm ex}+\kappa_0}$, where $\kappa_{\rm ex}$ describes the output coupling rate, whereas κ_0 denotes the intrinsic loss rate of the cavity.

The fields in the system's new eigenmodes

$$a_+ = (a_{\rm ccw} + a_{\rm cw})/\sqrt{2}, \tag{B3}$$

$$a_- = (a_{\rm ccw} - a_{\rm cw})/\sqrt{2} \tag{B4}$$

exert a radiation pressure force of

$$F_{\rm rp}(t) = -\hbar G(|a_+(t)|^2 + |a_-(t)|^2) \tag{B5}$$

since the spatial shape of the cross term $2{\rm Re}[a_+(t)a_-^*(t)]$ has an azimuthal dependence $\propto \cos(m\varphi)\sin(m\varphi)$ (m is the angular mode number of the whispering gallery mode), which averages to zero when projected on the azimuthally symmetric RBM. The coupled optomechanical equations of motion can therefore be written as

$$\dot{a}_+(t) = \left[i\left(\Delta - Gx(t) + \frac{\gamma}{2}\right) - \frac{\kappa}{2}\right]a_+(t) + \sqrt{\frac{\eta_{\rm c}\kappa}{2}}s_{\rm in}(t), \tag{B6}$$

$$\dot{a}_-(t) = \left[i\left(\Delta - Gx(t) - \frac{\gamma}{2}\right) - \frac{\kappa}{2}\right]a_-(t) + \sqrt{\frac{\eta_{\rm c}\kappa}{2}}s_{\rm in}(t), \tag{B7}$$

$$m_{\rm eff}\left[\ddot{x}(t)+\Gamma_{\rm m}\dot{x}(t)+\Omega_{\rm m}^2 x(t)\right] = -\hbar G[|a_+(t)|^2+|a_-(t)|^2]+\delta F(t), \quad \text{(B8)}$$

where $\delta F(t)$ is an external force, e.g., the thermal Langevin force.

We then apply the usual linearization

$$a_\pm(t)=\bar{a}_\pm+\delta a_\pm(t), \quad \text{(B9)}$$

$$x(t)=\bar{x}+\delta x(t) \quad \text{(B10)}$$

assuming $|\bar{a}_\pm| \gg |\delta a_\pm(t)|$ and $|\bar{x}| \gg |\delta x(t)|$. For the large mean occupancy of the modes and the mean mechanical displacement, we then obtain

$$\bar{a}_+ = \frac{\sqrt{\eta_{\rm c}\kappa/2}\,\bar{s}_{\rm in}}{-i(\bar{\Delta}+\gamma/2)+\kappa/2} =: \sqrt{\eta_{\rm c}\kappa/2}\,L_+(\bar{\Delta})\,\bar{s}_{\rm in}, \quad \text{(B11)}$$

$$\bar{a}_- = \frac{\sqrt{\eta_{\rm c}\kappa/2}\,\bar{s}_{\rm in}}{-i(\bar{\Delta}-\gamma/2)+\kappa/2} =: \sqrt{\eta_{\rm c}\kappa/2}\,L_-(\bar{\Delta})\,\bar{s}_{\rm in}, \quad \text{(B12)}$$

$$\bar{x} = -\frac{\hbar G}{m_{\rm eff}\Omega_{\rm m}^2}(|\bar{a}_+|^2+|\bar{a}_-|^2). \quad \text{(B13)}$$

The average displacement $\bar{x}$ induces a small static frequency shift, as does the (usually dominant) static shift due to absorption-induced heating [45], which are both absorbed into the mean detuning $\bar{\Delta}=\omega_{\rm l}-[\omega_{\rm c}(T)+G\bar{x}]$. One then obtains the equations of motion for small fluctuations,

$$\delta\dot{a}_+(t)=\left[i\left(\bar{\Delta}+\frac{\gamma}{2}\right)-\frac{\kappa}{2}\right]\delta a_+(t)-iG\bar{a}_+\delta x(t), \quad \text{(B14)}$$

$$\delta\dot{a}_-(t)=\left[i\left(\bar{\Delta}-\frac{\gamma}{2}\right)-\frac{\kappa}{2}\right]\delta a_-(t)-iG\bar{a}_-\delta x(t), \quad \text{(B15)}$$

$$m_{\rm eff}\left[\delta\ddot{x}(t)+\Gamma_{\rm m}\delta\dot{x}(t)+\Omega_{\rm m}^2\delta x(t)\right] = -\hbar G[\bar{a}_+^*\delta a_+(t)+\bar{a}_-^*\delta a_-(t)+\text{c.c.}]+\delta F(t). \quad \text{(B16)}$$

Fourier transformation gives

$$\delta a_+(\Omega) = \frac{-iG\bar{a}_+\delta x(\Omega)}{-i(\bar{\Delta}+\gamma/2+\Omega)+\kappa/2} = -iG\bar{a}_+\,L_+(\bar{\Delta}+\Omega)\,\delta x(\Omega), \quad \text{(B17)}$$

$$\delta a_-(\Omega) = \frac{-iG\bar{a}_-\delta x(\Omega)}{-i(\bar{\Delta}-\gamma/2+\Omega)+\kappa/2} = -iG\bar{a}_-\,L_-(\bar{\Delta}+\Omega)\,\delta x(\Omega), \quad \text{(B18)}$$

$$\delta x(\Omega)/\chi_{\rm m}(\Omega) = -\hbar G[\bar{a}_+^*\delta a_+(+\Omega)+\bar{a}_-^*\delta a_-(+\Omega)+\text{c.c.}]+\delta F(\Omega), \quad \text{(B19)}$$

with

$$\chi_{\rm m}(\Omega)=\frac{1}{m_{\rm eff}\left(-\Omega^2-i\Omega\Gamma_{\rm m}+\Omega_{\rm m}^2\right)}. \quad \text{(B20)}$$

Solving equations (B17)–(B19) for δx yields

$$\delta x(\Omega)=\frac{\delta F(\Omega)}{1/\chi_{\rm m}(\Omega)-i\hbar G^2(|\bar{a}_+|^2\{L_+(\bar{\Delta}+\Omega)-[L_+(\bar{\Delta}-\Omega)]^*\}+|\bar{a}_-|^2\{L_-(\bar{\Delta}+\Omega)-[L_-(\bar{\Delta}-\Omega)]^*\})}, \quad \text{(B21)}$$

so that we can write

$$\frac{1}{\chi_{\rm eff}(\Omega)}=\frac{1}{\chi_{\rm m}(\Omega)}-i\hbar G^2(|\bar{a}_+|^2\{L_+(\bar{\Delta}+\Omega)-[L_+(\bar{\Delta}-\Omega)]^*\}+|\bar{a}_-|^2\{L_-(\bar{\Delta}+\Omega)-[L_-(\bar{\Delta}-\Omega)]^*\}) \quad \text{(B22)}$$

and, in the regime of weak optomechanical coupling [32], the effective susceptibility is still approximately Lorentzian with a damping rate and resonance frequency given by

$$\Gamma_{\rm eff}\approx\Gamma_{\rm m}+2x_{\rm zpf}^2G^2{\rm Re}(|\bar{a}_+|^2\{L_+(\bar{\Delta}+\Omega)-[L_+(\bar{\Delta}-\Omega)]^*\}+|\bar{a}_-|^2\{L_-(\bar{\Delta}+\Omega)-[L_-(\bar{\Delta}-\Omega)]^*\}), \quad \text{(B23)}$$

$$\Omega_{\rm eff}\approx\Omega_{\rm m}+x_{\rm zpf}^2G^2{\rm Im}(|\bar{a}_+|^2\{L_+(\bar{\Delta}+\Omega)-[L_+(\bar{\Delta}-\Omega)]^*\}+|\bar{a}_-|^2\{L_-(\bar{\Delta}+\Omega)-[L_-(\bar{\Delta}-\Omega)]^*\}). \quad \text{(B24)}$$

APPENDIX C: CALCULATION OF THE IMPRECISION-BACKACTION PRODUCT

In the context of quantum measurements [46], it is interesting to characterize the sources of noise responsible for the mechanical displacement measurement uncertainty. For a given mechanical spectra, the measured (double-sided, symmetrized) spectral density of displacement fluctuations is given by

$$S_{xx}^{\rm meas}(\Omega)=S_{xx}^{\rm imp}(\Omega)+|\chi_{\rm eff}(\Omega)|^2S_{FF}(\Omega), \quad \text{(C1)}$$

where $S_{xx}^{\rm imp}(\Omega)$ describes the measurement imprecision due to apparent displacement fluctuations, which are actually caused by noise in the displacement transducer itself. $S_{FF}(\Omega)$ is the force noise acting on the mechanical oscillator, and $\chi_{\rm eff}(\Omega)$ its effective mechanical susceptibility. It is particularly interesting to evaluate these quantities for the lowest occupancy obtained at the optimum detuning of $\bar{\Delta}=-\Omega_{\rm m}-\frac{\gamma}{2}$ and at the Fourier frequency $\Omega=\Omega_{\rm m}$.

In our experiment, the *measurement imprecision* is dominated by shot noise, and we extract a value of

$$S_{xx}^{\rm imp}\equiv S_{xx}^{\rm imp}(\Omega_{\rm m})=(3.2\times10^{-19}\ {\rm m}/\sqrt{\rm Hz})^2$$

from the fit to the background of the recorded mechanical spectrum as shown in Fig. 4. Its measured linear dependence on the laser input power $P_{\rm in}$ shows that it is strongly dominated by the quantum noise of the input laser. This behavior is indeed expected at the frequencies of interest in our work, where classical quadrature fluctuations are negligible in Ti:sapphire lasers.

The thermal force noise (for $\frac{k_B T}{\hbar \Omega_m} \gg 1$) driving the mechanical oscillator is given by

$$S_{FF}^{\text{the}} \equiv S_{FF}^{\text{the}}(\Omega_m) = 2 m_{\text{eff}} k_B T \Gamma_m(T), \tag{C2}$$

which is given by the fluctuation-dissipation theorem. In the presence of dynamical backaction, we can estimate this force noise from the more directly measured linewidth Γ_{eff} and noise temperature T_{eff} using $T_{\text{eff}} \approx T \cdot \Gamma_m(T)/\Gamma_{\text{eff}}$, and

$$S_{FF}^{\text{the}} \approx 2 m_{\text{eff}} k_B T_{\text{eff}} \Gamma_{\text{eff}}. \tag{C3}$$

It evaluates to

$$S_{FF}^{\text{the}} = [(8 \pm 2) \times 10^{-15}\ \text{N}/\sqrt{\text{Hz}}]^2,$$

where Γ_{eff} and T_{eff} are extracted from the fits to the detuning series, evaluated at the detuning $\bar{\Delta} = -\Omega_m - \frac{\gamma}{2}$ as described in the main part of this article. This value gives a conservative estimate of the *classical measurement backaction*, considering effectively *all force noise* present in the system (including thermal noise due to the nonzero cryostat temperature) as a classical backaction of the measurement.

A less conservative estimate on the backaction of the actual displacement measurement using the laser coupled to the WGM can be made by separating two different contributions in the force noise,

$$S_{FF}^{\text{the}} = S_{FF}^{\text{cryo}} + S_{FF}^{\text{ba}}, \tag{C4}$$

where S_{FF}^{cryo} is the Langevin force noise due to the finite cryostat temperature T_{cryo} and S_{FF}^{ba} is the thermal backaction in the form of excess Langevin force noise due to the heating of the cavity by laser light. S_{FF}^{ba} gives an estimate of the classical perturbation of the system by the measurement, the *classical excess backaction*, which is technically avoidable.

The thermal force noise originating from the bath

$$S_{FF}^{\text{cryo}} = 2 m_{\text{eff}} k_B T_{\text{cryo}} \Gamma_m(T_{\text{cryo}}) \tag{C5}$$

is estimated to

$$S_{FF}^{\text{cryo}} = [(5 \pm 1) \times 10^{-15}\ \text{N}/\sqrt{\text{Hz}}]^2.$$

T_{cryo} and $\Gamma_m(T_{\text{cryo}})$ are extracted from independent low input power measurements where the RBM is thermalized to the cryostat temperature.

Consequently, the excess classical backaction evaluates to

$$S_{FF}^{\text{ba}} = [(6 \pm 2) \times 10^{-15}\ \text{N}/\sqrt{\text{Hz}}]^2$$

and accounts for 60% of the thermal force fluctuations driving the mechanical oscillator.

In addition to classical backaction, the quantum fluctuations of the intracavity photon number give rise to a *quantum measurement backaction* for which the force noise is given by

$$S_{FF}^{\text{qba}} \equiv S_{FF}^{\text{qba}}(\Omega_m) \approx \frac{2\hbar G^2 P_{\text{in}} \eta_c}{\bar{\omega}_c \Omega_m^2} = \frac{4 g_0^2 m_{\text{eff}} P_{\text{in}} \eta_c}{\bar{\omega}_c \Omega_m} \tag{C6}$$

in the case of high-resolved sideband factor $\frac{\Omega_m}{\kappa} \gg 1$ [18] and at the detuning of interest. It is of the order of $(1 \times 10^{-15}\ \text{N}/\sqrt{\text{Hz}})^2$ in our case, which is negligible compared to the classical backaction.

Therefore, a conservative estimate of the *imprecision-backaction product* is given by (for $\frac{k_B T}{\hbar \Omega_m} \gg 1$)

$$\sqrt{S_{xx}^{\text{imp}} \left(S_{FF}^{\text{the}} + S_{FF}^{\text{qba}}\right)} \approx \sqrt{S_{xx}^{\text{imp}} S_{FF}^{\text{the}}} = (49 \pm 8)\frac{\hbar}{2}.$$

In an ideal quantum measurement [46], this product is equal to $\frac{\hbar}{2}$, corresponding to the optimal compromise between quantum imprecision and quantum backaction, both arising from the quantum fluctuations of the optical field quadratures.

As it is shown in the main part of this article, laser absorption heating, which is responsible for the classical excess backaction S_{FF}^{ba}, is mainly caused by scattered light off the tapered fiber being absorbed by the toroid (in our case, by dust particles on the tapered fiber originating from particles in the air of our laboratory). It is, thus, within technical reach to strongly reduce this effect and perform measurements for which light-induced backaction would be dominated by quantum fluctuations.

[1] K. C. Schwab and M. L. Roukes, Phys. Today **58**, 36 (2005).
[2] T. J. Kippenberg and K. J. Vahala, Science **321**, 1172 (2008).
[3] F. Marquardt and S. M. Girvin, Physics **2**, 40 (2009).
[4] I. Favero and K. Karrai, Nat. Photonics **3**, 201 (2009).
[5] P. Rabl, S. J. Kolkowitz, F. H. L. Koppens, J. G. E. Harris, and M. D. Lukin, Nat. Phys. **6**, 602 (2010).
[6] A. D. O'Connell *et al.*, Nature (London) **464**, 697 (2010).
[7] V. B. Braginsky and A. B. Manukin, Sov. Phys. JETP **52**, 986 (1967).
[8] M. I. Dykman, Fizika Tverdogo Tela **20**, 2264 (1978).
[9] C. Höhberger Metzger and K. Karrai, Nature (London) **432**, 1002 (2004).
[10] A. Schliesser, P. Del'Haye, N. Nooshi, K. J. Vahala, and T. J. Kippenberg, Phys. Rev. Lett. **97**, 243905 (2006).
[11] O. Arcizet, P.-F. Cohadon, T. Briant, M. Pinard, and A. Heidmann, Nature (London) **444**, 71 (2006).
[12] S. Gigan, H. R. Böhm, M. Paternosto, F. Blaser, G. Langer, J. B. Hertzberg, K. C. Schwab, D. Bäuerle, M. Aspelmeyer, and A. Zeilinger, Nature (London) **444**, 67 (2006).
[13] T. Corbitt, Y. Chen, E. Innerhofer, H. Muller-Ebhardt, D. Ottaway, H. Rehbein, D. Sigg, S. Whitcomb, C. Wipf, and N. Mavalvala, Phys. Rev. Lett. **98**, 150802 (2007).
[14] D. Leibfried, R. Blatt, C. Monroe, and D. Wineland, Rev. Mod. Phys. **75**, 281 (2003).
[15] I. Wilson-Rae, N. Nooshi, W. Zwerger, and T. J. Kippenberg, Phys. Rev. Lett. **99**, 093901 (2007).
[16] M. Bhattacharya and P. Meystre, Phys. Rev. Lett. **99**, 073601 (2007).
[17] F. Marquardt, J. P. Chen, A. A. Clerk, and S. M. Girvin, Phys. Rev. Lett. **99**, 093902 (2007).
[18] A. Schliesser, O. Arcizet, R. Rivière, G. Anetsberger, and T. J. Kippenberg, Nat. Phys. **5**, 509 (2009).

[19] Y.-S. Park and H. Wang, Nat. Phys. **5**, 489 (2009).
[20] S. Gröblacher, J. B. Hertzberg, M. R. Vanner, S. Gigan, K. C. Schwab, and M. Aspelmeyer, Nat. Phys. **5**, 485 (2009).
[21] T. J. Kippenberg, H. Rokhsari, T. Carmon, A. Scherer, and K. J. Vahala, Phys. Rev. Lett. **95**, 033901 (2005).
[22] A. Schliesser and T. J. Kippenberg, in *Advances in Atomic, Molecular and Optical Physics*, edited by E. Arimondo, P. Berman, and C. C. Lin (Elsevier, New York, 2010), Vol. 58, Chap. 5.
[23] A. Schliesser, R. Rivière, G. Anetsberger, O. Arcizet, and T. J. Kippenberg, Nat. Phys. **4**, 415 (2008).
[24] G. Anetsberger, R. Rivière, A. Schliesser, O. Arcizet, and T. J. Kippenberg, Nat. Photonics **2**, 627 (2008).
[25] O. Arcizet, R. Rivière, A. Schliesser, G. Anetsberger, and T. J. Kippenberg, Phys. Rev. A **80**, 021803(R) (2009).
[26] M. Gorodetsky, A. Schliesser, G. Anetsberger, S. Deléglise, and T. J. Kippenberg, Opt. Express **18**, 23236 (2010).
[27] S. Weis, R. Rivière, S. Deléglise, E. Gavartin, O. Arcizet, A. Schliesser, and T. J. Kippenberg, Science **300**, 1520 (2010).
[28] C. Enss and S. Hunklinger, *Low Temperature Physics* (Springer, Berlin, 2005).
[29] W. A. Phillips, Rep. Prog. Phys. **50**, 1657 (1987).
[30] J. Jaeckle, Z. Phys. **257**, 212 (1972).
[31] R. Vacher, E. Courtens, and M. Foret, Phys. Rev. B **72**, 214205 (2005).
[32] J. M. Dobrindt, I. Wilson-Rae, and T. J. Kippenberg, Phys. Rev. Lett. **101**, 263602 (2008).
[33] D. S. Weiss, V. Sandoghdar, J. Hare, V. Lefèvre-Seguin, J. M. Raimond, and S. Haroche, Opt. Lett. **20**, 1835 (1995).
[34] T. J. Kippenberg, S. M. Spillane, and K. J. Vahala, Opt. Lett. **27**, 1669 (2002).
[35] V. B. Braginsky, S. E. Strigin, and V. P. Vyatchanin, Phys. Lett. A **287**, 331 (2001).
[36] C. Fabre, M. Pinard, S. Bourzeix, A. Heidmann, E. Giacobino, and S. Reynaud, Phys. Rev. A **49**, 1337 (1994).
[37] S. Mancini and P. Tombesi, Phys. Rev. A **49**, 4055 (1994).
[38] P. Verlot, A. Tavernarakis, T. Briant, P.-F. Cohadon, and A. Heidmann, Phys. Rev. Lett. **104**, 133602 (2010).
[39] K. W. Murch, K. L. Moore, S. Gupta, and D. M. Stamper-Kurn, Nat. Phys. **4**, 561 (2008).
[40] S. Gröblacher, K. Hammerer, M. R. Vanner, and M. Aspelmeyer, Nature (London) **460**, 724 (2009).
[41] L. Pauling, Phys. Rev. **36**, 430 (1930).
[42] S. Hunklinger, W. Arnold, S. Stein, R. Nava, and K. Dransfeld, Phys. Lett. A **42**, 253 (1972).
[43] R. O. Pohl, X. Liu, and E. Thompson, Rev. Mod. Phys. **74**, 991 (2002).
[44] H. A. Haus, *Waves and Fields in Optoelectronics* (Prentice-Hall, Englewood Cliffs, NJ, 1984).
[45] T. Carmon, L. Yang, and K. J. Vahala, Opt. Express **12**, 4742 (2004).
[46] V. B. Braginsky and F. Y. Khalili, *Quantum Measurement* (Cambridge University, Cambridge, UK, 1992).